A wintertime uptake window for anthropogenic CO_2 in the North Pacific

Keith B. Rodgers,[1] Jorge L. Sarmiento,[1] Olivier Aumont,[2] Cyril Crevoisier,[3] Clement de Boyer Montégut,[4] and Nicolas Metzl[5]

Received 31 December 2006; revised 13 September 2007; accepted 26 December 2007; published 31 May 2008.

[1] An ocean model has been forced with NCEP reanalysis fluxes over 1948–2003 to evaluate the pathways and timescales associated with the uptake of anthropogenic CO_2 over the North Pacific. The model reveals that there are two principal regions of uptake, the first in the region bounded by 35–45°N and 140–180°E, and the second along a band between 10–20°N and between 120°W and 180°E. For both of these regions, the dominant timescale of variability in uptake is seasonal, with maximum uptake occurring during winter and uptake being close to zero or slightly negative during summer when integrated over the basin. A decadal trend toward increased uptake of anthropogenic CO_2 consists largely of modulations of the uptake maximum in winter. For detection of anthropogenic changes, this implies that in situ measurements will need to resolve the seasonal cycle in order to capture decadal trends in ΔpCO_2. As uptake of anthropogenic CO_2 occurs preferentially during winter, observationally based estimates which do not resolve the full seasonal cycle may result in underestimates of the rate of uptake of anthropogenic CO_2. There is also a sizable circulation-driven decadal trend in the seasonal cycle of sea surface ΔpCO_2 for the North Pacific, with maximum changes found near the boundary separating the subtropical and subpolar gyres in western and central regions of the basin. These changes are due to a trend in the large-scale circulation of the gyres, which itself is driven by a trend in the wind stress over the basin scale. This trend in the three-dimensional circulation is more important than the local trend in mixed layer depth (MLD) in contributing to the decadal trend in ΔpCO_2.

Citation: Rodgers, K. B., J. L. Sarmiento, O. Aumont, C. Crevoisier, C. de Boyer Montégut, and N. Metzl (2008), A wintertime uptake window for anthropogenic CO_2 in the North Pacific, *Global Biogeochem. Cycles*, *22*, GB2020, doi:10.1029/2006GB002920.

1. Introduction

[2] Because of burning of fossil fuels and cement production, in the mid-1990s approximately 6.6 Petagrams of carbon per year (Pg C/a) were being released to the atmosphere. Of this, approximately 3.3 Pg remained in the atmosphere [*Keeling and Piper*, 2000], another 2.2 ± 0.4 Pg were being absorbed by the oceans [*Sabine et al.*, 2004], and a residual of 1.1 Pg are thought to have entered the terrestrial biosphere. However, from observations very little is known about how these fluxes into the oceanic and terrestrial carbon reservoirs vary in time, or what the main rate-limiting processes are for uptake of anthropogenic CO_2. Developing a better understanding of the time variability will be important to understanding how the system adjusts to global warming.

[3] Although our interests are in the global ocean, this study focuses on using a state-of-the-art ocean circulation model to study the timescales and pathways that characterize the uptake of anthropogenic CO_2 for the North Pacific. The ocean uptake of anthropogenic CO_2 was first addressed using three-dimensional circulation models in the studies of *Maier-Reimer and Hasselmann* [1987], *Bacastow and Maier-Reimer* [1990], and *Sarmiento et al.* [1992]. These early studies could not address variability in uptake as they were forced with time-invariant fields at the sea surface. Since the appearance of these papers, a range of ocean modeling studies have addressed interannual variability in air-sea CO_2 fluxes [*Winguth et al.*, 1994; *Le Quéré et al.*, 2000; *Obata and Kitamura*, 2003; *McKinley et al.*, 2004; *Wetzel et al.*, 2005]. Variability in air-sea CO_2 fluxes over the North Pacific was also evaluated for seven models in an intercomparison study of *McKinley et al.* [2006]. Among the studies that have considered interannual variability in air-sea CO_2 fluxes, only that of *Wetzel et al.* [2005] has explicitly addressed the anthropogenic component of CO_2. Nevertheless, the study of *Wetzel et al.* [2005] was largely

[1] Atmospheric and Ocean Sciences, Princeton University, Princeton, New Jersey, USA.
[2] Centre IRD de Bretagne, Plouzané, France.
[3] Laboratoire de Météorologie Dynamique, CNRS, IPSL, Ecole Polytechnique, Paliseau, France.
[4] Frontier Research Center for Global Change (FRCGC), JAMSTEC, Yokohama Institute for Earth Sciences, Yokohama, Kanagawa, Japan.
[5] LOCEAN/IPSL, UMR 7159, Université Pierre et Marie Curie, Paris, France.

0886-6236/08/2006GB002920$12.00

descriptive and did not directly concern itself with physical processes.

[4] The present study was in large part motivated by the data analysis study of *Takahashi et al.* [2006], which used in situ measurements to characterize the decadal trend in the rate of change of sea surface ΔpCO_2 (here defined as the difference between the atmospheric partial pressure of CO_2 and sea surface pCO_2) over the North Pacific over 1970–2004. There it was argued that the decadal trend in ΔpCO_2 over much of the open area regions of the North Pacific is close to zero, although there are some deviations around the margins of the subpolar gyre. Although the *Takahashi et al.* [2006] study offers a significant step forward in describing changes from observations, there are two important questions that cannot be addressed from the observational record alone. The first issue is a separation of the observed ΔpCO_2 trend into the component due to the anthropogenic perturbation and the component due to a decadal trend in ocean circulation. To what extent are the associated patterns and amplitudes of the respective patterns different? Developing a framework for distinguishing between these components will be important for the purpose of detecting the anthropogenic signal. The second issue which cannot be addressed from observations alone is the extent to which the decadal trend in sea surface ΔpCO_2 is different when considered separately for winter and summer conditions. Winter conditions are rather poorly represented in the historical database, and it is important to identify what (if any) biases this introduces in estimating decadal trends. Such biases could also have ramifications for estimates of the rate of uptake of CO_2 by the North Pacific.

[5] Additionally, we are interested in using a model to interpret the data presented in the study of *Dore et al.* [2003], where pCO_2 measurements for ocean station ALOHA (22°45′N, 158°W) were evaluated over 1989–2002. There it was shown that the decadal trend in ΔpCO_2 was negative over this period. This behavior is not resolved in the basin-scale analysis of *Takahashi et al.* [2006], although this may in part be due to the fact that the time intervals considered for the two studies are not identical. As their study did not include a model, *Dore et al.* [2003] could only speculate on the mechanism driving the negative trend in ΔpCO_2, and they argued that it is due to changes in the local freshwater fluxes at the sea surface. In a subsequent study, *Keeling et al.* [2004] used output from a physical circulation model to motivate a discussion of potential mechanisms. However, as the model simulation considered did not include the carbon cycle, they were not able to establish the specific mechanism controlling the changes.

[6] Here we use a state-of-the-art ocean model that includes an ocean biogeochemistry/food web model to address the uptake of anthropogenic CO_2 for the North Pacific. We have chosen a model configuration that includes two separate ocean DIC tracers, one that maintains a constant preanthropogenic atmospheric CO_2 concentrations as a boundary condition and the other which uses the anthropogenic atmospheric transient. Thus the difference between these representations of ocean carbon and air-sea fluxes give us an explicit representation of the anthropogenic signal.

[7] Our primary goals in this study are to use an ocean model to address the following questions: (1) Where is anthropogenic CO_2 entering the North Pacific Ocean? (2) Is there a strong seasonal variability to the uptake of anthropogenic CO_2? (3) What is the relative amplitude and structure of the components of the decadal trend in ΔpCO_2 due to the anthropogenic transient in atmospheric CO_2 and to a decadal trend in ocean circulation, and what are the mechanisms that control these different components? and (4) What is the amplitude of seasonal variations in the full air-sea CO_2 fluxes, and how much do they contribute to the observed amplitude of atmospheric CO_2 variations at Mauna Loa?

[8] This paper is organized as follows: We begin with an analysis of the ocean model simulations of sea surface ΔpCO_2 and air-sea CO_2 fluxes. Consideration is given to the spatial structures of variability, as well as the temporal characteristics of variability. We then present an analysis of the physical state variables in order to identify the dynamical controls on sea surface ΔpCO_2 variations. We then discuss the results we obtained using an atmospheric transport model that used the ocean model–generated air-sea CO_2 fluxes as a lower boundary condition to evaluate the atmospheric CO_2 concentration response at Mauna Loa to the ocean model fluxes.

2. Model Description

2.1. Description of Ocean Circulation and Ocean Biogeochemistry Models

[9] The ocean circulation model used for this study is the ORCA2 configuration of the Ocean Parallelisé (OPA) version 8.1 [*Madec et al.*, 1998]. The model domain is global, with horizontal resolution of approximately 2° in the extratropics, and meridional resolution enhanced to 0.5° in the vicinity of the equator. The model uses 30 vertical levels, with 20 of these in the upper 500 m. Horizontal mixing is oriented along isopycnal surfaces, and the parameterization of *Gent and McWilliams* [1990] for mesoscale eddies is used poleward of 10° latitude in either hemisphere. Vertical mixing is achieved using the TKE scheme of *Blanke and Delecluse* [1993]. The model employs a free surface [*Roullet and Madec*, 2000]. The biogeochemical model used is the Pelagic Interaction Scheme for Carbon and Ecosystem Studies (PISCES), which is described in detail by *Aumont and Bopp* [2006]. The carbon chemistry in the model follows OCMIP-2 protocols (http://www.ipsl.jussieu.fr/OCMIP/phase2/), and gas exchange is performed using the paramaterization of *Wanninkhof* [1992].

[10] The surface momentum forcing fields are taken from the daily mean wind stress fields from the NCEP-1 reanalysis [*Kalnay et al.*, 1996] over the period 1948–2003. As such, the physical model configuration and forcing are identical to that used in the study of *Rodgers et al.* [2004]. Surface heat fluxes are calculated using bulk formulas. The surface air temperature and air humidity from the NCEP reanalysis are used in the calculation of surface heat fluxes. Freshwater fluxes at the ocean surface are calculated using the evaporative fluxes from bulk formulas in conjunction with the precipitation fluxes from NCEP

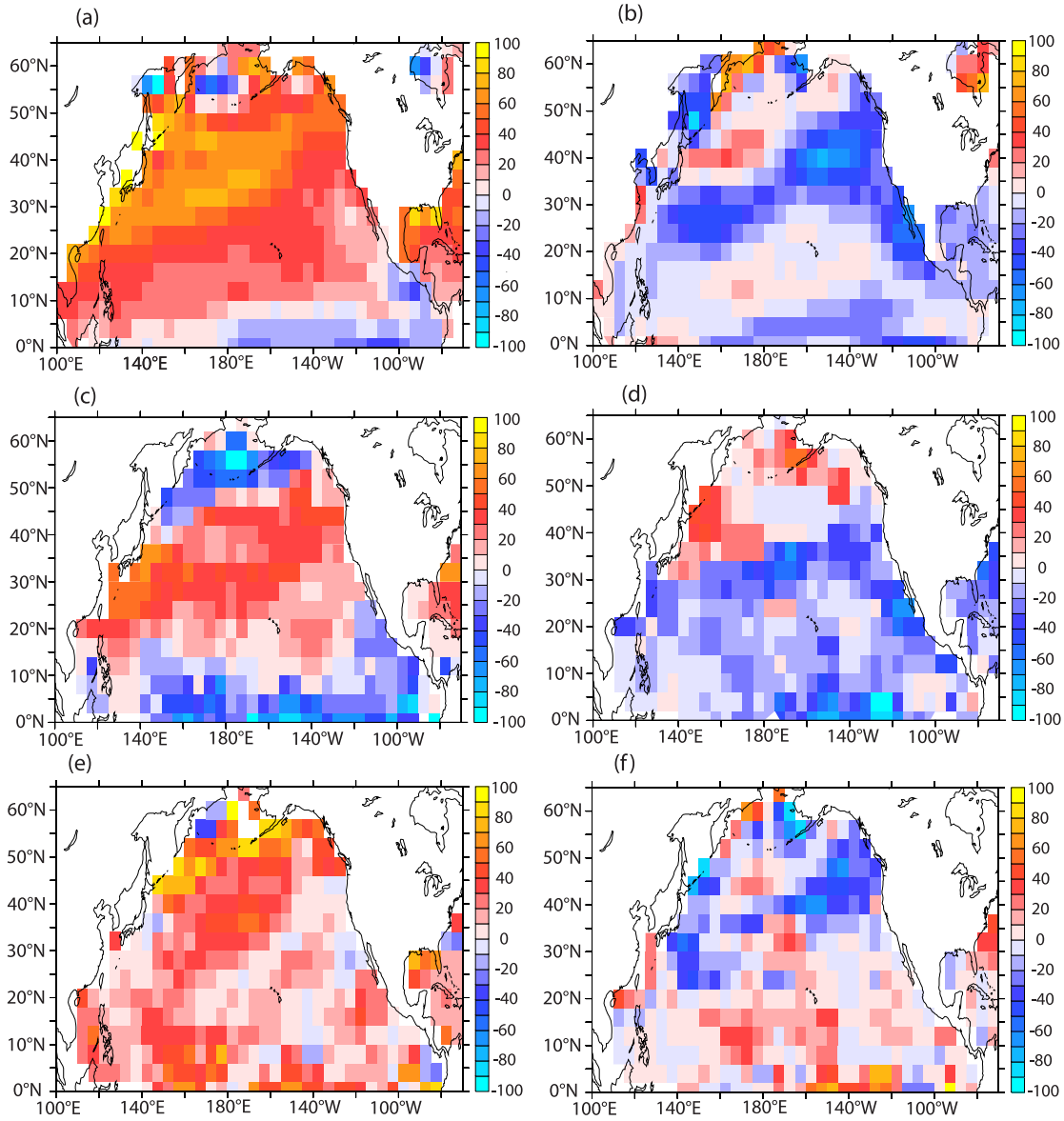

Figure 1. Maps of sea surface ΔpCO_2 (pCO_{2atm} minus pCO_{2oce}) (μatm). (a) February 1995 from the PISCINT experiment. (b) August 1995 from the PISCINT experiment. (c) February 1995 from climatology of *Takahashi et al.* [2002]. (d) August 1995 from climatology of *Takahashi et al.* [2002]. (e) Difference: PISCINT minus climatological data product for February 1995. (f) Difference: PISCINT minus climatological data product for August 1995.

(1948–1979) and *Xie and Arkin* [1997] over the period 1979–2003. The model's free surface boundary condition is formulated such that ocean volume is globally conserved, as is the total salinity content of the ocean. Thus "nudging" of sea surface salinity is performed through a restoring flux of freshwater into the surface layer, with an equivalent time-scale of relaxation of 12 d for the 10-m-thick surface layer (to the monthly climatology of *Boyer et al.* [1998]). In this way, the salt content of the ocean is globally conserved. However, given that the global volume integral of the freshwater flux associated with the restoring freshwater flux is not zero, there is drift in the globally averaged sea surface height.

2.2. Experimental Configuration for Ocean Model

[11] Two separate simulations are considered with ORCA2-PISCES, and they differ only in the boundary condition used for atmospheric CO_2. The two runs have been analyzed for the Atlantic in the study of *Raynaud et al.* [2006]. The first experiment is denoted by PISCES Inter-annual (PISCINT) for which the atmospheric transient in CO_2 is used over 1765–2003. The second simulation, PISCES Control (PISCCTL), maintains pre-anthropogenic

atmospheric levels of 280 ppm for the atmospheric boundary condition. For both simulations, the calculations are performed offline over the period 1765–1947 with climatological (i.e., a repeating seasonal cycle) circulation fields, and then online over 1948–2003 with interannually varying circulation fields. The evolving physical state of the ocean is identical for both PISCINT and PISCCTL. In our evaluation of the model output fields, we consider the difference between the PISCINT and PISCCTL experiments. As biology in the PISCES model is not DIC-limited, the biological pump behaves effectively identically for the two experiments, so that differences between the two runs can be attributed to solubility.

[12] This study includes an analysis of mixed layer depth (MLD) and a comparison with observations [*de Boyer Montégut et al.*, 2004]. Given that there are many more temperature than salinity profiles available for the North Pacific, we have chosen to use a temperature-based criterion (a temperature difference of 0.2°C from the near-surface value at 10-m depth) for our evaluation of MLD in the observations and the model. Climatological and interannually varying fields from 1950 to 2005 were generated using all available high vertical resolution hydrographic profiles, including Mechanical BathyThehrmograph (MBT), expendable BathyThermograph (XBT), Conductivity-Temperature-Depth (CRTD), and profiling floats. The data (approximately 4.7 million profiles) were obtained from the National Oceanographic Data Center and the World Ocean Circulation Experiment (WOCE) databases.

2.3. Transport Model Description

[13] We also use the MOZART-2 [*Horowitz et al.*, 2003] atmospheric transport model with the model-derived air-sea CO_2 fluxes over 1990–2003 to evaluate the effect of these fluxes on the seasonal to interannual timescale variability in the atmospheric CO_2 time series. NCEP reanalysis circulation fields are used to drive the MOZART-2 model (an evaluation of model performance using SF6 is presented by *Gloor et al.* [2007]). In the MOZART-2 model, advection is based on the semi-Lagrangian scheme of *Lin and Rood* [1996] and includes a pressure correction developed by P. Cameron-Smith to ascertain tracer mass flux conservation. Convective mass fluxes are rediagnosed by MOZART-2 using the *Hack* [1994] scheme for shallow and midconvection and the *Zhang and McFarlane* [1995] scheme for deep convection. Vertical diffusion within the planetary boundary layer is represented using the parameterization of *Holstlag and Boville* [1993].

3. Results

3.1. Comparison of Modeled ΔpCO_2 With Observations

[14] We begin our analysis with a consideration of the seasonal cycle in ΔpCO_2 (defined as the difference between the partial pressure of atmospheric CO_2 and the pCO_2 at the sea surface) for the North Pacific. The February 1995 ΔpCO_2 for the PISCINT experiment (Figure 1a) is positive over nearly all of the North Pacific, for which case the gradient would drive a net flux of CO_2 into the ocean. Maximum values tend to lie in the western and central regions of the basin. The August 1995 ΔpCO_2 distribution for PISCINT (Figure 1b) is negative over much of the basin, with a local minimum stretching diagonally across the basin from 25°N, 155°W to 40°N, 155°W.

[15] The ΔpCO_2 distribution for the 1995 climatology of *Takahashi et al.* [2002] is shown for February (Figure 1c) and August (Figure 1d). This observational climatology reveals that the wintertime ΔpCO_2 is somewhat too large for the PISCINT simulation, with better agreement occurring during summer. To highlight the model biases, the difference between PISCINT and the data product is shown for February in Figure 1e and for August in Figure 1f. Clearly, the biases are most pronounced in February in the subpolar gyre and in the central regions of the subtropical gyre, with the bias having the same sign over nearly the entire North Pacific. The model biases are weaker during summer, with a region of maximum bias in the region bounded by 160°W–130°W, 35°N–50°N. This analysis thus establishes that the model reproduces important characteristics of the seasonal variability in ΔpCO_2 represented in the data product of *Takahashi et al.* [2002], and thereby this modeling configuration is an appropriate tool for addressing the relationship between seasonal variations and the uptake of anthropogenic CO_2.

3.2. Spatial and Temporal Characteristics of the Uptake of Anthropogenic CO_2

[16] Next we are interested in evaluating the pathways by which anthropogenic CO_2 enters the ocean and, once in the ocean, where it is stored. The air-sea flux of CO_2 integrated over 1993–2001 for the PISCINT experiment is shown in Figure 2a, with positive values indicating a net flux into the ocean. The years 1993 and 2001 are chosen arbitrarily, as they correspond to the sampling interval of Repeat Hydrography (in this case, of WOCE P17N in 1993 and CLIVAR P17N in 2001) where we address variability in oceanic DIC and O_2 inventories. However, the main results shown here are not very sensitive to the particular dates chosen for the time interval and hold generally for the sampling frequency of the CLIVAR Repeat Hydrography program. The flux into the ocean is maximum in the northern subtropical gyre region and in the subpolar gyre, with a local maximum extending from 140°E to 170°W between 35–45°N. Fluxes out of the ocean are found along the coast of the Americas to the south of 30°N, with maximum outgassing occurring between 5°N and 10°S to the east of 160°E and along the eastern boundary to the south of the equator. The equivalent field for the PISCCTL simulation is shown in Figure 2b, with this being the model representation of the natural CO_2 flux in the absence of the anthropogenic perturbation in atmospheric CO_2 concentration. Here the flux into the North Pacific can be seen to be weaker than is the case for PISCINT, whereas the equatorial outgassing is stronger.

[17] The uptake of anthropogenic CO_2 over the same period, taken as the difference between the fluxes from the PISCINT and PISCCTL experiments, is shown in Figure 2c. This field exhibits two maxima in the North Pacific, one centered around 40°N between 140°E and 180°E, and the second along a band between 10–20°N,

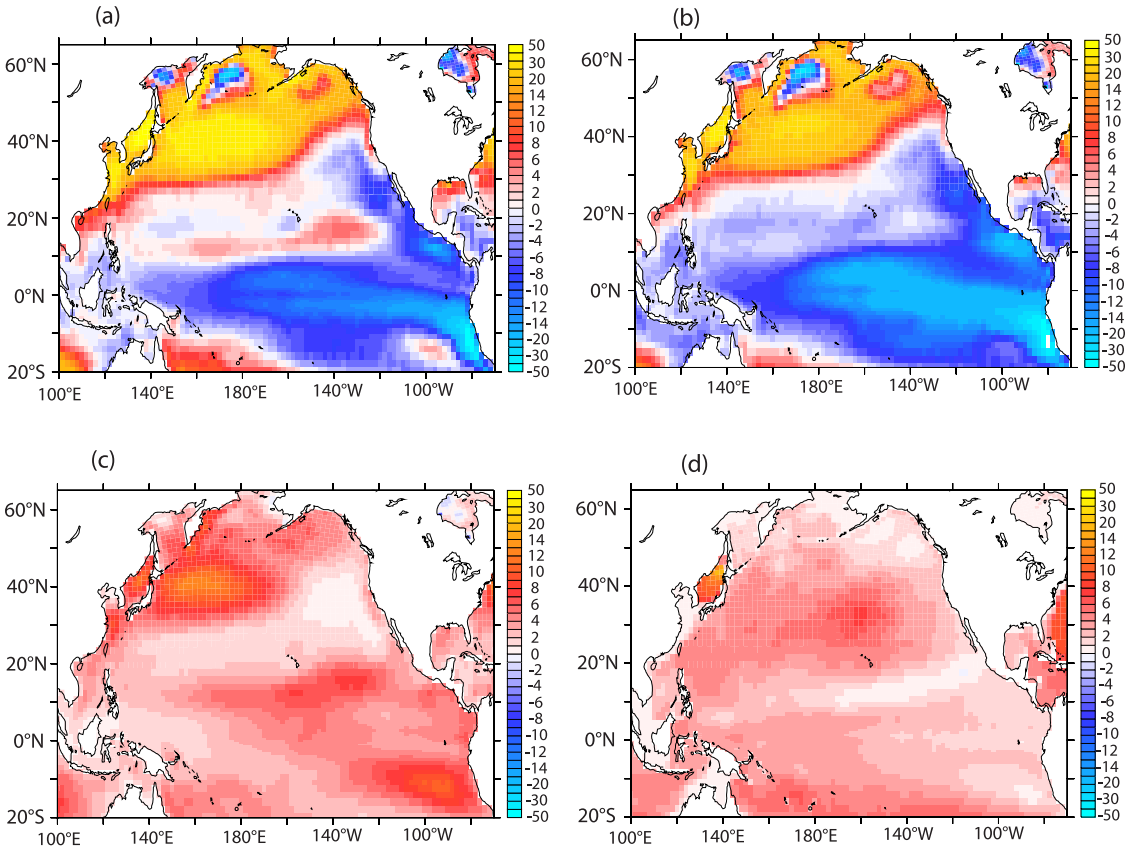

Figure 2. Uptake and inventories. (a) Air-sea CO_2 flux integrated over 1993–2001 for PISCINT (moles/m^2) with positive values indicating flux into the ocean. (b) Air-sea CO_2 flux integrated over 1993–2001 for PISCCTL (moles/m^2) with positive values indicating flux into the ocean. (c) Uptake of perturbation CO_2 via gas exchange (moles/m^2) integrated over 1993–2001. (d) Change in vertical inventory of perturbation DIC between 1993 and 2001 (PISCINT minus PISCCTL) (moles/m^2).

extending from 180°E to 120°W. Both of these maxima in the anthropogenic uptake correspond to maxima for the total integrated flux in the PISCINT experiment (Figure 2a). The change in the vertically integrated anthropogenic DIC inventory (the difference between the PISCINT and PISCCTL experiments) between 1993 and 2001 is shown in Figure 2c. This shows that for the ocean inventories there is a maximum accumulation of anthropogenic DIC over this period in the center of the subtropical gyre to the north of Hawaii.

[18] In Figure 3a, the monthly time series of air-sea CO_2 fluxes integrated over the North Pacific (5–65°N) are shown for both the PISCINT experiment (black) and the PISCCTL experiment (red). In Figure 3, positive fluxes correspond to a net flux of CO_2 from the atmosphere into the ocean. Figure 3 reveals that the fluxes have a very strong seasonal component, with relatively strong uptake in winter and weaker outgassing in summer. Both experiments reveal the same seasonal phase. The difference between the two time series (PISCINT minus PISCCTL) is shown in Figure 3b and corresponds to the rate of uptake of anthropogenic CO_2 over the North Pacific (5–65°N). The uptake of anthropogenic CO_2 is occurring with a pronounced seasonality, with maximum uptake occurring predominantly during winter. The rate of uptake increases over the course of the experiment, with the increase characterized by an amplification of the seasonal cycle. The increase in uptake is modulated by interannual variations in the uptake rate, and these modulations are most clearly evident during winter. Modulations (i.e., interannual variability) are relatively weak until approximately 1990. In the early 1990s, there is a reduction in the rate of increase in winter uptake, and this is followed by a maximum in uptake in the winter of 1997/1998, during the largest El Niño in the instrumental record. However, no striking "decadal shifts" in uptake are associated with either the 1976/1977 or 1997/1998 shifts in the phase of the Pacific Decadal Oscillation, and this is consistent with what was found in the model intercomparison study of *McKinley et al.* [2006] for the total CO_2 flux. By the last decade of the simulation, the peak rate of uptake during winter is slightly less than 0.8 Gt C/a.

[19] In Figure 3c, the monthly uptake of anthropogenic CO_2 shown in Figure 3 is decomposed into two regions, the latitude range 25–65°N and the latitude range 5–25°N. Additionally, the same field with a 12-month running mean is shown for the northern region and the southern region. For both regions the seasonal variability occurs in phase,

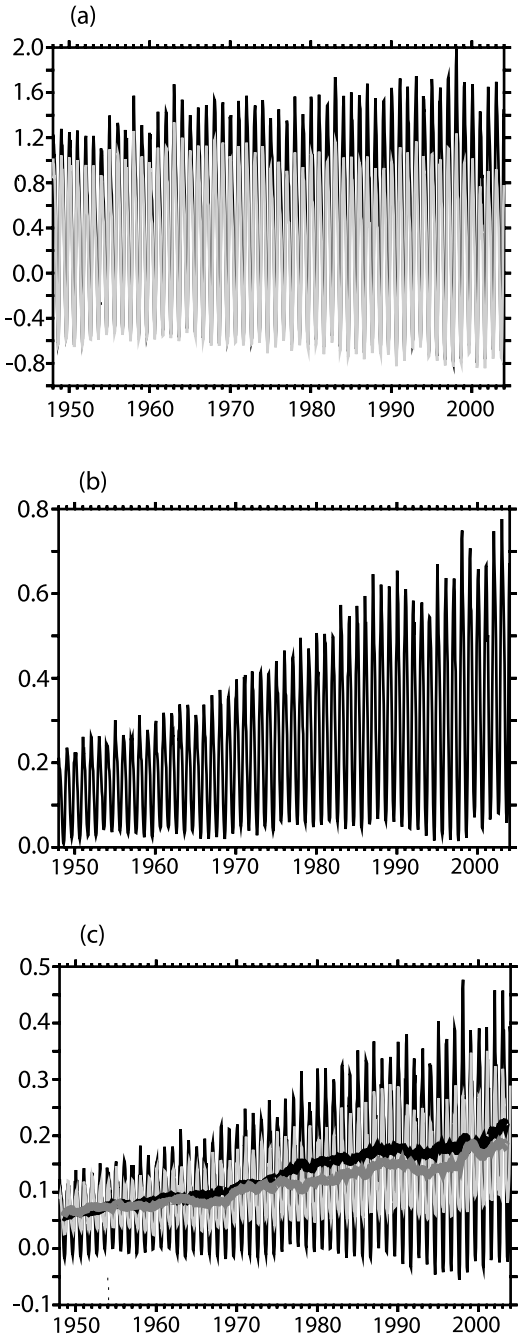

Figure 3. Time series showing the evolution of integrated quantities over the North Pacific. (a) Monthly basin-integrated (5–65°N) air-sea CO_2 fluxes for PISCINT (black) and PISCCTL (gray) (Pg C/a). (b) Basin-integrated (5–65°N) uptake of anthropogenic CO_2 (PISCINT minus PISCCTL) (Pg C/a). (c) Anthropogenic flux by region: 25–65°N (black); 5–25°N (gray); 25–65°N with a 1-year running mean (bold black); and 5–25°N with a 1-year running mean (bold gray).

with uptake that is maximum during winter. However, the amplitude of the seasonal variations is significantly larger for the northern region, where there is weak outgassing of anthropogenic CO_2 occurring during some summers. As for decadal changes, Figure 3c reveals that the integrated uptake for the two regions of approximately the same amplitude until the mid-1970s, after which the tendency is for the uptake in the northern region to be approximately 25% larger than the uptake in the southern region. For neither region is a significant "decadal" shift found.

3.3. Decadal Trends in Sea Surface ΔpCO_2

[20] Next we evaluate whether decadal trends in ΔpCO_2 are different for wintertime and summertime conditions considered separately, as this could have important implications for detection of anthropogenic change. The linear trend in annual mean ΔpCO_2 over 1970–2000 for PISCINT (Figure 4a) reveals alternating regions of positive and negative trends in ΔpCO_2. Positive/negative values indicate that the rate of increase of sea surface pCO_2 is smaller/larger than the rate of increase of atmospheric CO_2 concentration. Not surprisingly, in the equatorial Pacific where there is strong upwelling, and in the Kuroshio Extension region, where there is enhanced vertical mixing, the trend in ΔpCO_2 is positive. This is due to the fact that subsurface waters in these regions were last in contact with the atmosphere at a time when atmospheric CO_2 concentrations were lower, and therefore when these subsurface waters are entrained into the surface mixed layer they carry with them a memory of lower atmospheric CO_2 concentration. This causes the sea surface pCO_2 to lag the rate of increase of atmospheric CO_2 concentration in these regions of enhanced physical exchange between surface and subsurface waters.

[21] Next we evaluate the extent to which the decadal trend presented in Figure 4a is different when considered separately for wintertime and summertime conditions. The linear trend in winter (February) ΔpCO_2 values over the period 1970–2000 is shown in Figure 4b. For the North Pacific, the positive ΔpCO_2 trend in the Kuroshio Extension region as well as in the western and eastern subpolar gyres is significantly larger in winter than for the annual mean, which is not surprising considering that winter is the season where there tends to be enhanced exchange between surface and subsurface waters.

[22] The linear trend in sea surface ΔpCO_2 for summer (August) over 1970–2000 for PISCINT is shown in Figure 4c and reveals that in summer the ΔpCO_2 trend over the Kuroshio Extension region (40°N–45°N) are negative, such that the sea surface pCO_2 is increasing more rapidly than the atmospheric concentration of CO_2. In fact, on the basin scale, a large contiguous structure where the trend in ΔpCO_2 is negative can be seen to extend across the band 40–45°N between 140°E and 140°W, and at 140°W it connects to an arc which extends southwestward toward approximately 170°E, 25°N.

[23] Taken together, the disparate trends in ΔpCO_2 for February and August indicate an increase in the seasonal cycle of ΔpCO_2 over 1970–2000. This is considered explicitly in Figure 4d, which shows the absolute value of the difference between the August trend (Figure 4c) and the February trend (Figure 4b) for PISCINT. The increased seasonality in sea surface ΔpCO_2 exhibits a distinct maximum over much of the northern subtropics as well as the

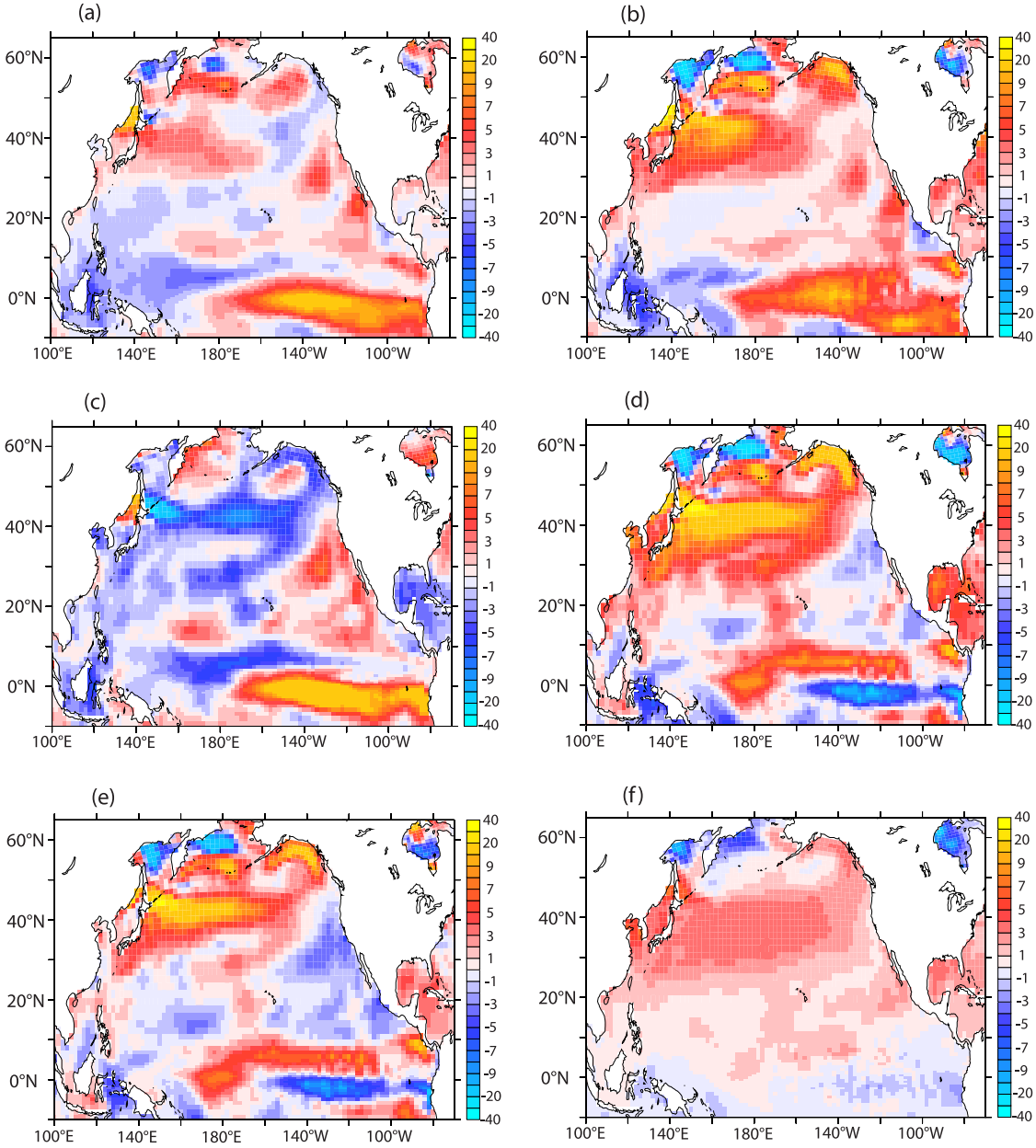

Figure 4. Evaluation of decadal trends in ΔpCO_2 for ORCA2-PISCES (μatm/decade). (a) Annual mean trend in ΔpCO_2 over 1970–2000 for PISCINT. (b) Trend in February ΔpCO_2 over 1970–2000 for PISCINT. (c) Trend in August ΔpCO_2 over 1970–2000 for PISCINT. (d) Trend in amplitude of seasonal cycle for PISCINT (Figure 4c minus Figure 4b). (e) Same as Figure 4d except for PISCCTL (circulation component). (f) Difference (Figure 4d minus Figure 4e): noncirculation component of trend in seasonal cycle.

subpolar region, with values as large as 20 μatm/decade stretching across 40°N.

[24] What is controlling the very large increase in the seasonal cycle of ΔpCO_2 over 1970–2000 for PISCINT? To answer this we consider the linear trend in the amplitude of the seasonal cycle for ΔpCO_2 over the same period for PISCCTL in Figure 4e. There the boundary condition for atmospheric CO_2 concentration was maintained at preindustrial levels, and thus any decadal trend in the amplitude of the seasonal cycle for ΔpCO_2 must be controlled by variability in circulation. The pattern in Figure 4e captures most of the large-amplitude features found for PISCINT in Figure 4d, in particular the extrema in the northern subtropics and the subpolar regions. This clearly demonstrates that most of the basin-scale structure seen in Figure 4d is due to a trend in the circulation of the ocean.

[25] The residual decadal trend in the amplitude of the seasonal cycle in sea surface ΔpCO_2 over 1970–2000,

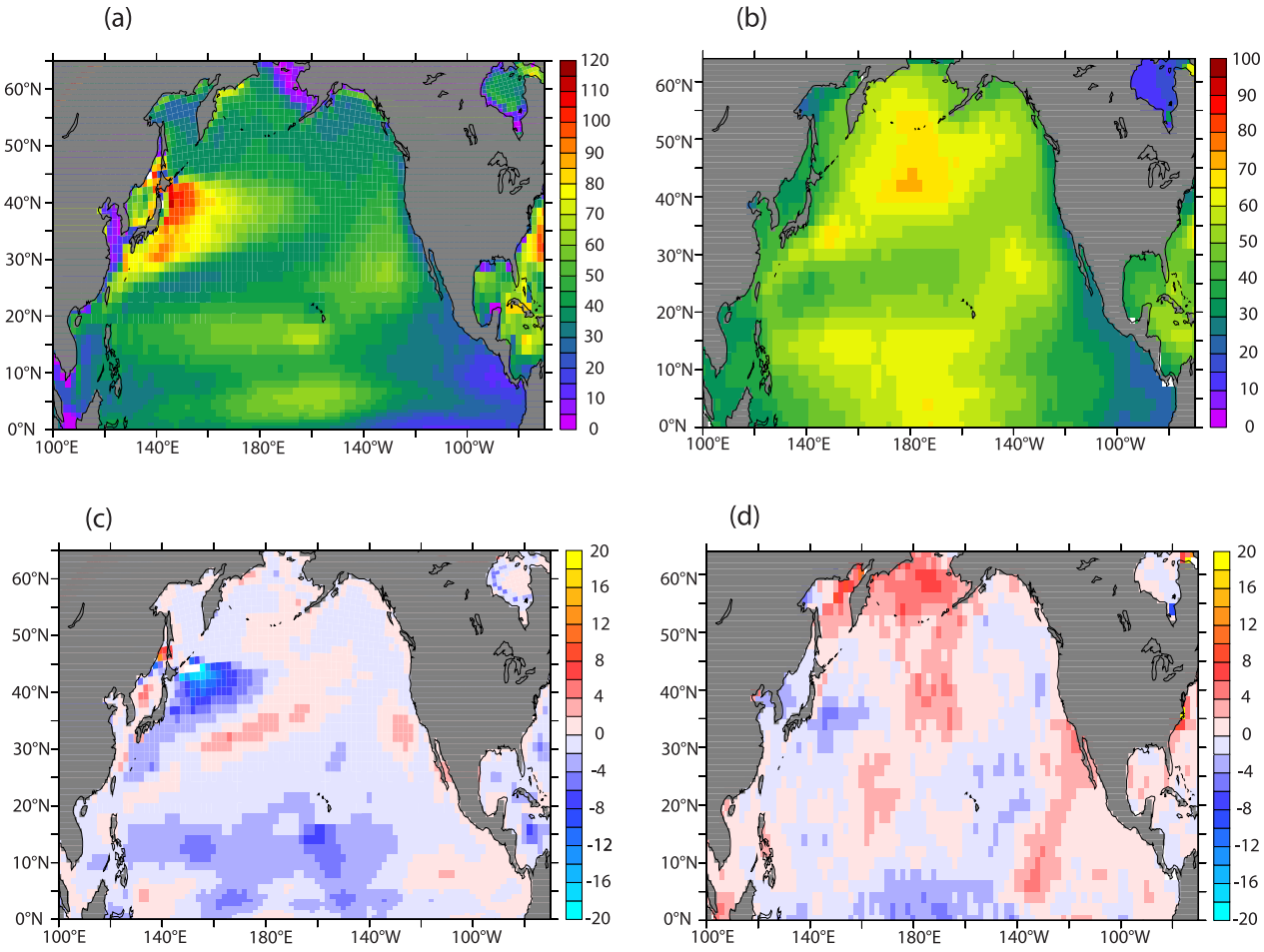

Figure 5. Mixed layer depth, or MLD (defined using a 0.2°C temperature criterion as described in text). (a) Annual mean MLD for PISCINT (PISCCTL is identical) (m). (b) Annual mean MLD from the data product of *de Boyer Montégut et al.* [2004] using temperature criterion (m). (c) Decadal MLD trend for PISCINT (m/decade). (d) Decadal MLD trend for data product of *de Boyer Montégut et al.* [2004] (m/decade).

namely the difference between the trends for PISCINT (Figure 4d) and PISCCTL (Figure 4e), is shown in Figure 4f. For this residual, the effects of circulation have been removed from the decadal trend in seasonality for PISCINT, thereby leaving the response in the seasonal cycle of ΔpCO_2 that one would expect for a steady ocean circulation field in response to the secular trend in the atmospheric CO_2 boundary condition. This reveals a maximum increase in the seasonal cycle over the open ocean in the central and western subtropical Pacific north of 25°N. This corresponds to the "uptake window" for anthropogenic CO_2 shown in Figure 2c.

3.4. Mean and Decadal Trends in the Physical State of the Ocean

[26] What dynamical mechanisms determine the position of the "uptake window" for anthropogenic CO_2 evident in Figure 2c? To evaluate this, we consider the mean MLD distribution for the model averaged over 1970–2000 in Figure 5a and the MLD from observations over the same period in Figure 5b. The model can be seen to exhibit a shallow bias in the subpolar gyre, as well as a shallow bias in the MLD maximum structure that follows the southern and southeastern reaches of the subtropical gyre. On the other hand, the model exhibits a bias toward a deep MLD relative to observations (by approximately 25–35%) in the Kuroshio Extension region.

[27] The modeled MLD maximum region corresponds to the position of the uptake window for CO_2 in Figure 2c. This is due to the fact that wintertime convection here for PISCINT accesses waters which were last at the surface during a time when atmospheric CO_2 concentrations were lower, and it is this state of disequilibrium with the higher atmospheric CO_2 that drives an anthropogenic flux of CO_2 revealed by the different between PISCINT and PISCCTL. It is this relationship between the large-scale structure of MLD and the uptake of anthropogenic CO_2 that is important here, and which is robust despite the model bias in MLD in relation to the observations in the North Pacific.

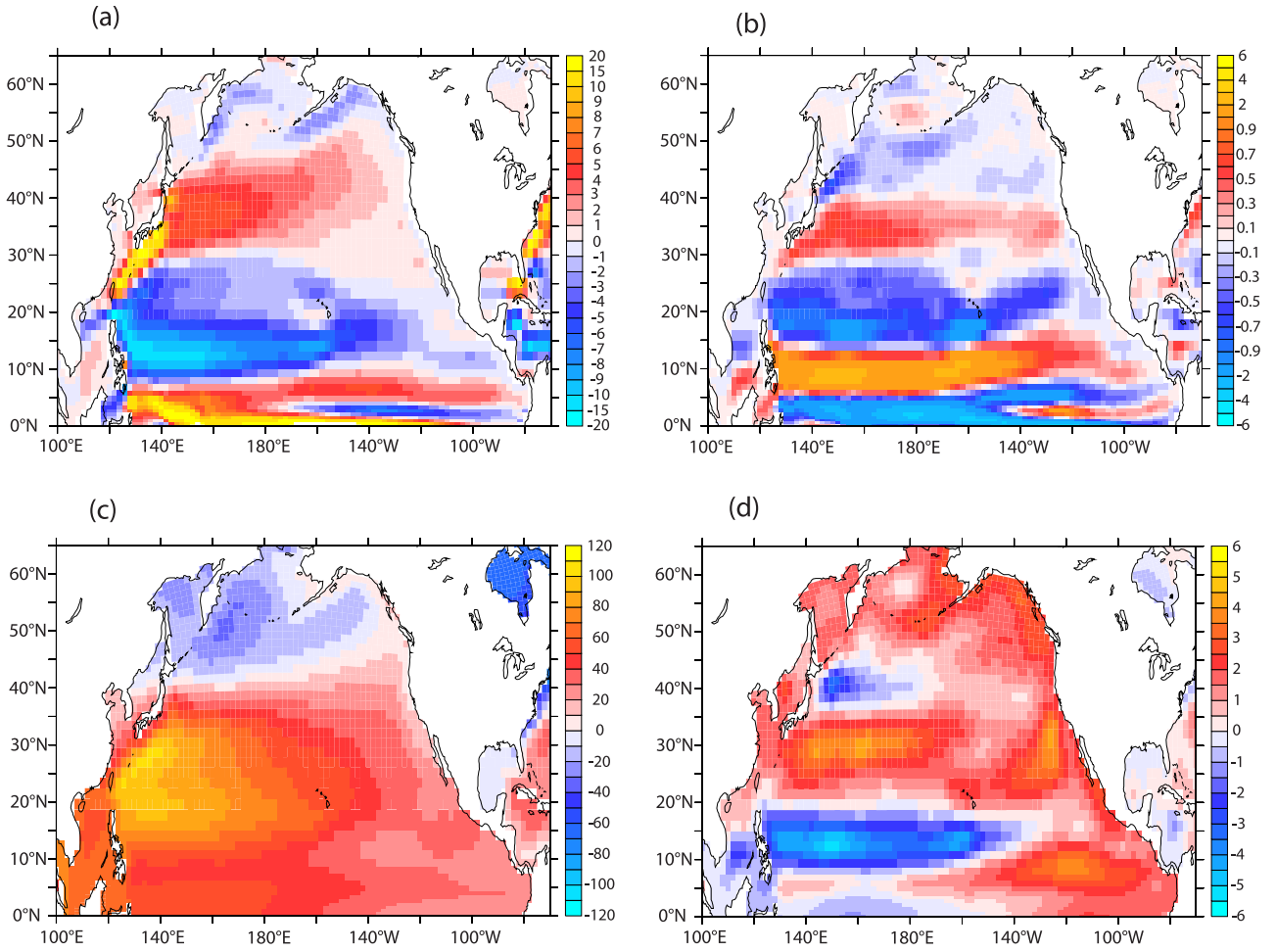

Figure 6. Circulation diagnostics for PISCINT simulation (identical for PISCCTL). (a) Mean zonal velocity averaged over the upper 400 m (u_{400}) over 1970–2000 (cm/s). (b) Linear trend in u_{400} over 1970–2000 (cm/s/decade). (c) Mean sea surface height (SSH) averaged over 1970–2000 (cm). (d) Linear trend in SSH over 1970–2000 (cm/decade).

[28] We next turn our attention to the dynamical processes that control the decadal trend in sea surface ΔpCO_2 for the PISCCTL run (Figure 4e), which we have seen is distinct from what is found for the uptake window. We begin with a consideration of the linear trend in the simulated MLD over 1970–2000 (Figure 5c) and the trend over the same period in the observations (Figure 5d). The model reveals a trend toward a shoaling of the MLD by 10 m/decade in the region directly to the east of Japan, but otherwise very close to zero over the central and eastern regions of the subtropics and throughout the subpolar regions. The observations, on the other hand, reveal a weak trend toward a shallower MLD of several meters per decade over the region to the east of Japan with this maximum structure extending southward into the central subtropical gyre. Thus although the pattern of the mean modeled MLD (Figure 5a) corresponds to the mean "uptake window" (Figure 2c), the decadal trend in MLD does not correspond closely to the decadal trend in ΔpCO_2 associated with changes in circulation (Figure 4e).

[29] What then is the dynamical control on the decadal trend in the seasonal amplitude of ΔpCO_2 for PISCCTL (Figure 4c)? We consider next for the model the zonal component of velocity averaged over the upper 400 m (u_{400}) for the period 1970–2000 in Figure 6a. This reveals the large-scale zonal component of the upper thermocline circulation with maximum eastward transport occurring over the latitude range 30–45°N (the model's Kuroshio Extension region), and maximum westward transport occurring over the latitude range 10–20°N (the model's North Equatorial Current). The linear trend in u_{400} over the period 1970–2000 is shown in Figure 6b, revealing a tendency toward enhanced eastward transport over 30–40°N and increased westward transport over 10–20°N. These changes constitute an increase in the strength of the rotation of the subtropical gyre over the period 1970–2000. Clearly, the decadal trend in u_{400} does not assume the same structure as the mean for u_{400}. The trend toward increased eastward transport over 30–40°N is counterbalanced by a trend toward slight weakening of the transport over 40–45°N.

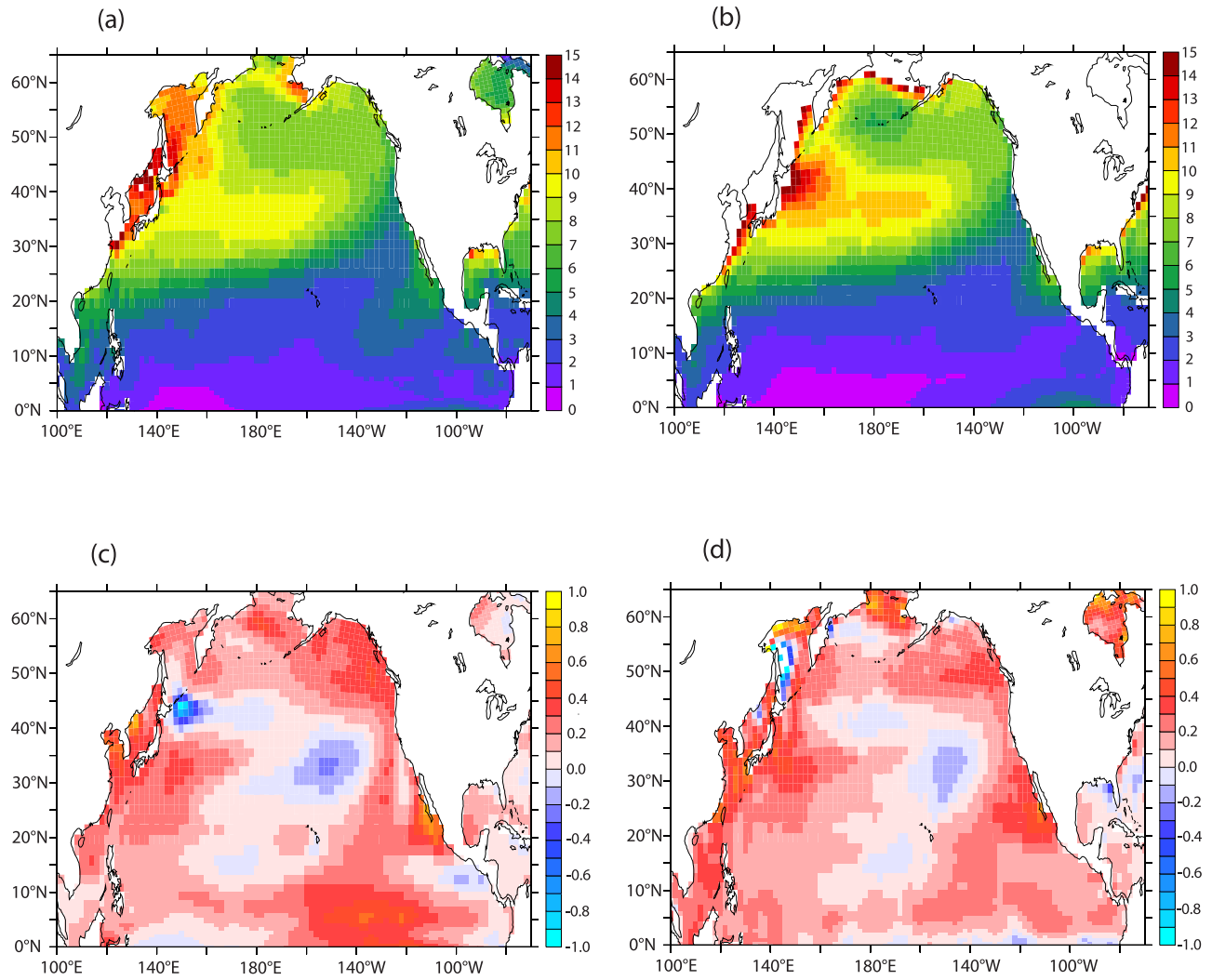

Figure 7. Sea surface temperature (SST) over 1970–2000 for PISCINT (identical for PISCCTL). (a) Amplitude of climatological seasonal cycle for model (°C). (b) Amplitude of climatological seasonal cycle for observations (°C). (c) Linear trend for PISCINT (°C/decade). (d) Linear trend for observations (°C/decade).

Thus the trend toward increased subtropical gyre strength is accompanied by a southward shift of the boundary separating the subpolar and subtropical gyres.

[30] To illustrate how these circulation fields are reflected in the large-sale structure of the gyre, the mean modeled sea surface height (SSH) over 1970–2000 is shown in Figure 6c. The u_{400} maxima in Figure 6a are clearly associated with regions where the meridional gradients in SSH are largest, consistent with near-geostrophic balance. The linear trend in SSH over the period 1970–2000 is shown in Figure 6d. This pattern is consistent with a strengthening of the subtropical gyre already seen in Figure 6b, with the maximum trend in zonal transports coincident with the maximum trend in meridional gradients in SSH. This serves to underscore that there is an equatorward shift in the boundary separating the subpolar and subtropical gyres in the western and central Pacific. The close correspondence of this diagnostic of changes in the gyre structure to the trend of the seasonal cycle in ΔpCO_2 associated with changes in circulation (Figure 4e) demonstrates that the trend in the gyre structure rather than the trend in MLD is driving the ΔpCO_2 changes in this region.

[31] Although the model has revealed the importance of changes in the seasonal cycle of ΔpCO_2 for understanding trends in ΔpCO_2 for the North Pacific, there are not sufficient pCO_2 measurements with which to constrain the simulated seasonal cycle on the basin scale. However, given the strong sensitivity of sea surface pCO_2 to changes in sea surface temperature (SST) [*Takahashi et al.*, 1993] and the fact that SST is well known from observations, it is important to evaluate whether the model exhibits any significant bias in its representation of SST. The amplitude of the climatological seasonal cycle in SST over 1970–2000 is shown for the model in Figure 7a and for the observations

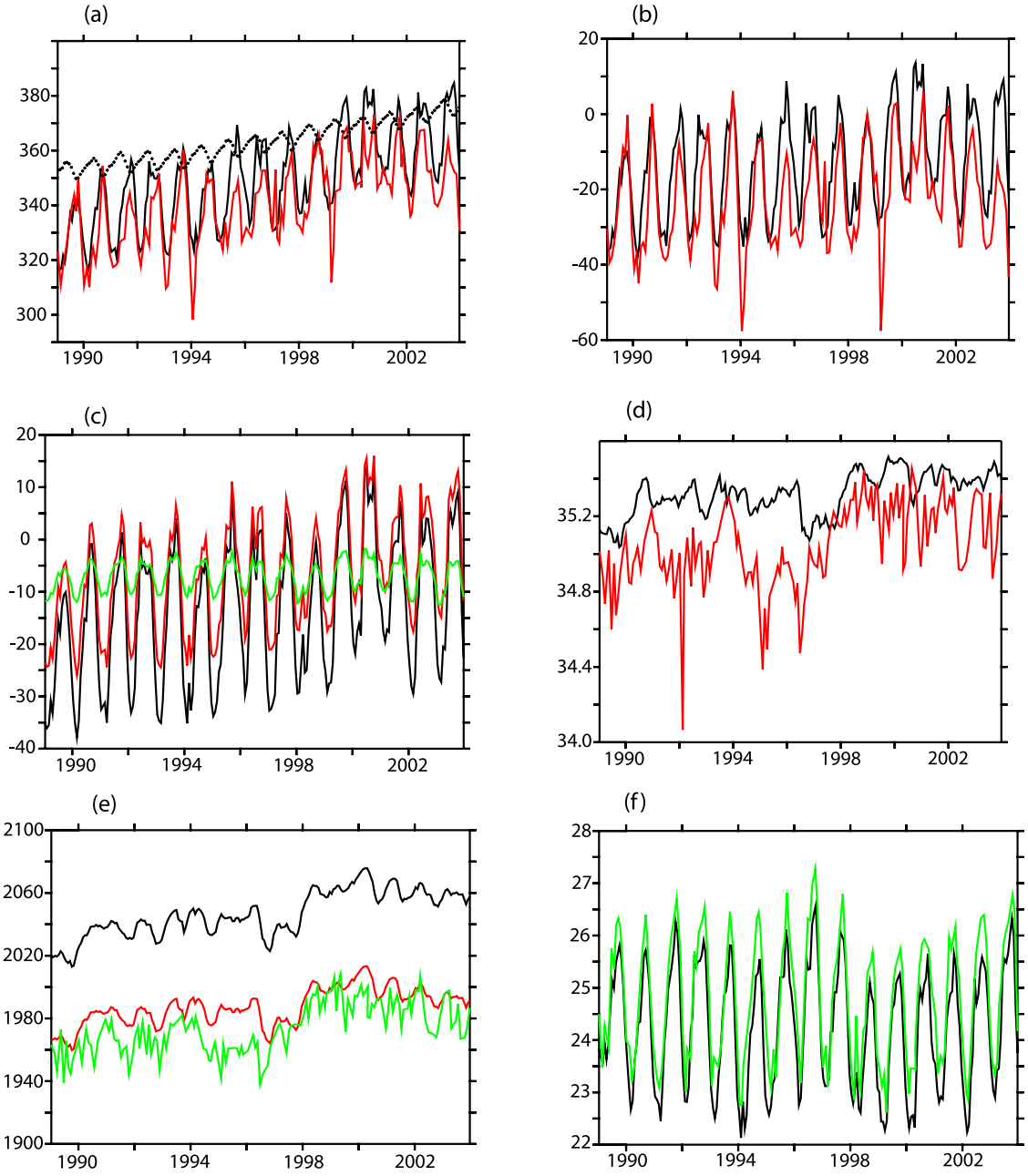

Figure 8. Comparison for sea surface of model with data of *Dore et al.* [2003] from ALOHA over 1989–2002: (a) pCO_2, with PISCINT (black), the observations (red), and atmospheric CO_2 concentrations at Mauna Loa shown (dots) (μatm); (b) ΔpCO_2 (oceanic minus atmospheric pCO_2), with PISCINT shown in black and the observations shown in red (μatm); (c) ΔpCO_2 with PISCINT (black), PISCCTL (red), and the difference (PISCINT minus PISCCTL) (bold green); (d) salinity for the model (black) and observations (red) (psu); (e) DIC for PISCINT (black), PISCCTL (red), and observations (bold green) (μmol/kg); and (f) SST for model (black) and observations (green) (°C).

in Figure 7b. Figures 7a and 7b reveal that over most of the North Pacific, the biases in the amplitude of SST variations are less than 10%, and they are still less than 20% in the western subpolar and subtropical regions. The linear decadal trend in SST is shown for the model in Figure 7c and for the observations in Figure 7d. The model is able to reproduce the observed decadal trend. Importantly, the pattern for the decadal trend in SST (Figure 7c) is distinct

from the pattern found for the decadal trend in sea surface ΔpCO_2 (Figure 4a).

3.5. Evaluation of Model Output for Ocean Station ALOHA

[32] Whereas the analysis of *Takahashi et al.* [2006] could not account for the high-frequency (seasonal) variations in their analysis of the decadal trend on a basin scale, the study of *Dore et al.* [2003] considered the evolution of the monthly sea surface pCO_2 at ocean station ALOHA (22°45′N, 158°W) over 1989–2002. The surface pCO_2 as simulated by the PISCINT experiment is compared with the observations in Figure 8a, along with both the observed sea surface pCO_2 and the atmospheric CO_2 concentration at Mauna Loa (shown as a series of dots). The model captures to first order the amplitude of the seasonal variations in pCO_2, although it is not able to capture some of the subseasonal variations, nor is it able to simulate the very low sea surface pCO_2 concentrations observed in 1994 and 1999. The modeled and simulated ΔpCO_2 (shown here as the difference between oceanic and atmospheric pCO_2) are compared over the same period in Figure 8b. The model is clearly consistent with the observations in showing an increase in ΔpCO_2, although the model can be seen to underrepresent the interannual modulations of the amplitude of the seasonal cycle of ΔpCO_2 for this site.

[33] In order to identify whether the decade-long trend toward increasing ΔpCO_2 for the model grid point corresponding to ALOHA is driven by variability in the surface forcing fields, the ΔpCO_2 over 1989–2002 is shown for PISCINT and PISCCTL in Figure 8c, with the difference between the two (PISCINT minus PISCCTL) overlain. The linear trends in ΔpCO_2 over this period for PISCINT and PISCCTL are 9.759 μatm/decade and 9.472 μatm/decade, respectively. Given that for PISCINT this trend can only be due to variability in the surface forcing fields, the fact that this decadal trend is so similar demonstrates that for PISCINT this trend is largely controlled by interannual variability in surface forcing. The difference between PISCINT and PISCCTL reveals the component of the variability in ΔpCO_2 that is due to the anthropogenic perturbation. This component reveals that the anthropogenic perturbation amplifies the seasonal cycle in ΔpCO_2, but that the amplitude of the amplification is rather steady over 1989–2002.

[34] Given that the linear decadal trend in ΔpCO_2 for PISCINT is controlled by variability in surface forcing, to what extent does the model support the hypothesis for this trend proposed by *Dore et al.* [2003], namely that it is driven by variability in surface freshwater fluxes, which then modify surface pCO_2 through modifications in surface salinity? The simulated and observed monthly variations in salinity for ALOHA are shown in Figure 8d. Because of the restoring boundary condition used for the model on sea surface salinity, the model greatly underestimates variability in sea surface salinity for this site. In particular, the model is not able to capture the shift from less salty to more salty conditions with the 1997/1998 El Niño event. Thus the fact that the model is able to capture the decadal trend toward increased ΔpCO_2 over 1989–2002 without changes in surface salinity indicates that this trend in ΔpCO_2 must be due to some other process.

[35] The modeled sea surface DIC concentrations (for both PISCINT and PISCCTL) are compared with the observations in Figure 8e. The PISCINT simulation reveals a bias toward concentrations that are too high by 60–70 μmol/kg relative to the observations. This bias in DIC is not reflected in surface pCO_2 as it is compensated by a high bias in surface alkalinity (not shown). Importantly, PISCCTL is able to capture the abrupt DIC concentration increase about the 1997/1998 El Niño event, and thereby these changes must be controlled by circulation changes. The modeled SST is compared with the observations in Figure 8f. Despite a persistent small cold bias of order 0.5°C, the model represents well the temporal structure of seasonal, interannual, and decadal changes in SST.

3.6. Calculation With Atmospheric Transport Model

[36] We have seen that the variability in the air-sea CO_2 fluxes when integrated over the basin scale is dominated by seasonal changes for the PISCINT and PISCCTL experiments (Figure 3a), and the same is true for both experiments in the North Atlantic (not shown). Here we consider results from the MOZART-2 atmospheric transport model in order to evaluate how the ocean model–derived fluxes impact the atmospheric concentration of CO_2. The fluxes from the PISCINT and PISCCTL experiments have been used as lower boundary conditions for MOZART-2 over 1990–2003, and the MOZART-2 model itself has been driven by atmospheric fields from the NCEP reanalysis [*Kalnay et al.*, 1996]. For convenience, the experiment with MOZART-2 using CO_2 fluxes from PISCINT will henceforth be referred to as ATM_PISCINT (with ATM being an acronym for Atmospheric Transport Model), and the experiment using fluxes from PISCCTL will be referred to as ATM_PISCCTL.

[37] The atmospheric concentrations for the surface model grid point corresponding to Mauna Loa are shown for ATM_PISCINT and ATM_PISCCTL in Figure 9a over 1994–2003, along with the observed CO_2 concentration for Mauna Loa. To facilitate interpretation, the evolving concentrations corresponding to ATM_PISCINT and ATM_PISCCTL are shown as deviations from the observed concentration for Mauna Loa in January 1994. The ATM_PISCINT experiment reveals a clear trend toward decreasing atmospheric CO_2 concentration over 1994–2003, reflecting the net uptake for PISCINT of 2.25–2.5 Pg C/a over this period. The trend is modulated by seasonal variations, with the amplitude and phase controlled largely by the winter uptake and summer outgassing over the oceans in the Northern Hemisphere. The ATM_PISCCTL curve shows a slight trend toward increasing CO_2 over this period, associated with a weak global outgassing of CO_2 over 1994–2003.

[38] The linearly detrended concentrations for ATM_PISCINT and ATM_PISCCTL are shown in Figure 9b, along with the detrended anthropogenic perturbation component (i.e., the difference between ATM_PISCINT and ATM_PISCCTL), as well as the detrended observed concentrations for Mauna Loa. The simulated seasonal cycle for the ATM_PISCINT experiment has an amplitude which is less

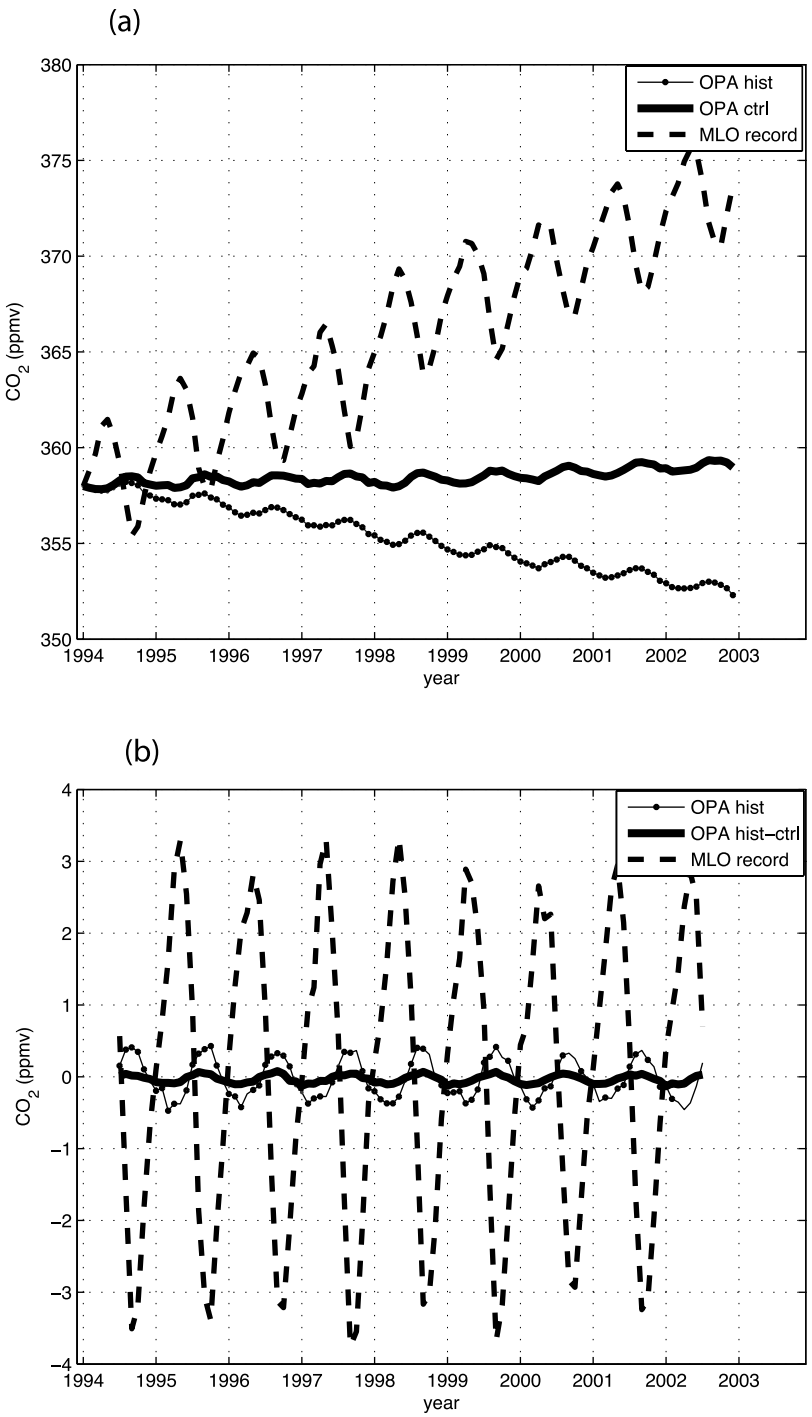

Figure 9. Output from the MOZART atmospheric transport model: (a) Comparison of simulated concentration at Mauna Loa for PISCINT (bold curve) and PISCCTL (thin curve), along with the observed concentration at Mauna Loa (dashed). (b) Detrended curves for the PISCINT simulation (bold curve), the difference between the PISCINT and PISCCTL experiments (thin curve), and the observed atmospheric CO_2 concentrations for Mauna Loa (dashed).

than 15% of that seen in the observed CO_2 concentrations, and it is approximately antiphased with relation to the observations. The amplitude of the detrended anthropogenic signal (i.e., the changes associated with the anthropogenic fluxes shown in Figure 3b) is very small, and thus according to this calculation it has very little effect on atmospheric CO_2 concentrations. There is almost no interannual variability in the ATM_PISCINT curve in Figure 9b, and this

model result implies that nearly all of the variance in observed CO_2 concentration is due to the terrestrial biosphere.

[39] It is not clear to what extent the air-sea flux variability in the model is underestimated because of biases associated with model resolution and physical parameterizations in the ORCA2 circulation model. Additionally, as the various tendency terms that contribute to variability of DIC concentration in the mixed layer (i.e., lateral advection versus vertical mixing, etc.) were not explicitly calculated as output diagnostics for PISCINT and PISCCTL, we are not able to quantitatively assess the relative roles of vertical mixing and shifts in frontal positions in influencing sea surface ΔpCO_2 variations.

4. Discussion

[40] Before proceeding to a general discussion of the results presented thus far, it is important to first briefly review an assumption implicit in our use of the phrase "anthropogenic perturbation" when referring to the difference between the CO_2 flux fields and oceanic DIC fields output from the PISCINT and PISCCTL experiments. In general, one would expect that in addition to the response to the secular trend in the atmospheric concentration of CO_2, there could be another component of the anthropogenic signal in oceanic DIC due to global warming–induced changes in ocean circulation, which itself could induce changes in surface CO_2 fluxes. The NCEP reanalysis fluxes used to force the PISCCTL experiment span 1948–2003, and there is as yet no unambiguous way of quantitatively separating the global warming and natural variability components of the decadal trends in the fluxes. In other words, for the linear trend in ΔpCO_2 over 1970–2000 for the PISCCTL experiment (Figure 4e) we know that the trend is due to changes in circulation, but we do not know to what extent those decadal changes in circulation are due to natural variability in circulation or to global warming. Thus in our use of the terminology "anthropogenic perturbation" we are implicitly assuming that the circulation changes themselves are due to natural variability in the climate system and that the global warming–induced changes are a second-order perturbation which can be ignored for this particular scientific question. Within this framework, the linear trend described in the circulation fields is assumed to be associated with low-frequency (decadal and longer) timescale variability.

[41] Through the combined use of the PISCINT and PISCCTL simulations, we were able to separate the decadal trend in the seasonal amplitude of ΔpCO_2 into the contribution driven by the component resulting from the decadal trend in ocean circulation (Figure 4e) and the anthropogenic perturbation in atmospheric CO_2 concentrations (Figure 4f). The model simulations revealed that the decadal trends for the two different components assume different spatial patterns and that they are controlled by different physical processes. The circulation-driven decadal trend in ΔpCO_2 also has a pattern that is distinct from the pattern of the decadal trends in SST, with the difference in air-sea equilibration timescales for pCO_2 and temperature contributing to these differences.

[42] The figure presenting the spatial pattern of uptake of anthropogenic CO_2 over the North Pacific (Figure 2c) reveals that there are two regions of maximum uptake, the larger being in the northwestern part of the subtropical gyre (the region bounded by 35–45°N, 140°–180°E), and a secondary maximum roughly following the southern flank of the subtropical gyre (the region bounded by 10–20°N, 180–110°W). This pattern is consistent with what has been found in previous studies [e.g., *Sarmiento et al.*, 1992]. The fact that the basin-integrated uptake increases over 1970–2000 is largely due to the decadal increases in the seasonal cycle of sea surface ΔpCO_2. In other words, it is the trend in wintertime ΔpCO_2 that increases the flux of CO_2 from the atmosphere into the ocean. The model/data comparison for ALOHA (Figure 8) demonstrated that the model is able to simulate the observed decadal changes in sea surface pCO_2 there between 1989 and 2001. Despite the high DIC concentration bias for the PISCINT and PISCCTL simulations, the model reproduces the amplitude of the observed abrupt shift in DIC concentrations in 1998 for both the PISCINT and PISCCTL simulations. This clearly demonstrates that the shift is due to variability in ocean circulation, supporting the interpretation of ALOHA data presented by *Keeling et al.* [2004].

[43] Nevertheless, the model does exhibit a bias toward a seasonal cycle in ΔpCO_2 that is too large on the basin scale, with the bias being larger in winter (Figure 1e) than during summer (Figure 1f). What processes or biases in physical state variables could contribute to this bias in ΔpCO_2? The seasonal cycle in SST (Figures 7a and 7b) is relatively well represented in the model, and is itself unlikely to be responsible for the bias in ΔpCO_2. However, the simulated MLD does tend to be too shallow throughout the subpolar gyre and the central subtropics between 170°E and 140°E, and this corresponds to the important regions of a high model bias in wintertime ΔpCO_2 (Figure 1e).

[44] We have emphasized here that the decadal trend toward a southward shift in the position of the boundary separating the subtropical and subpolar gyres emphasized acts as a circulation control on the decadal trend in seasonal ΔpCO_2 variations. This decadal trend in circulation itself is consistent with the findings of the previous ocean modeling studies of *Seager et al.* [2001] and *Yasuda and Sakurai* [2006]. *Yasuda and Sakurai* [2006] used ocean model sensitivity studies to show that this type of decadal trend is determined by the wind stress patterns over the basin scale. MLD variations, on the other hand, are controlled by variations in stratification, local freshwater fluxes, and local heat fluxes which themselves can be related to local variations in wind speed. For this reason, the processes controlling MLD are in important ways uncoupled from the processes driving shifts in gyre boundaries.

[45] The model results here do have some potentially important implications for deciding which analysis methods are appropriate for understanding the relationship between variations of pCO_2 and the variations of other variables.

This is often done by starting from the differential thermodynamic expression for $dpCO_2$ in the form introduced by *Takahashi et al.* [1993]:

$$dpCO2 = (\partial pCO2/\partial SST) * dSST + (\partial pCO2/\partial DIC) * dDIC + (\partial pCO2/\partial ALK) * dALK + (\partial pCO2/\partial SSS) * dSSS$$

where the partial derivative terms are found empirically (and where SST, DIC, ALK, and SSS are the local sea surface temperature, DIC concentration, alkalinity, and sea surface salinity, respectively). This expression is well suited for small equilibrated perturbations in closed systems. It should however not be assumed that this applies to regions where shifting fronts are associated with first-order changes in water mass characteristics and biogeochemical properties. Yet these are precisely the regions where sea surface ΔpCO_2 variations may be largest. We leave as a subject for future study a detailed process-focused investigation of dynamical controls on carbon cycle variability in gyre boundary/frontal regions.

[46] Calculations performed with the MOZART atmospheric transport model illustrated that the seasonal CO_2 concentration response at Mauna Loa to the air-sea CO_2 fluxes from the PISCINT experiment over 1994–2003 was slightly less than 1 ppmv. This response is to a total seasonal cycle of Northern Hemispheric ocean flux variability of approximately 3.6 Gt C/a, and thus the scaling of the atmospheric response is approximately a 0.25 ppmv response to a 1.0 Gt C/a seasonal cycle in air-sea CO_2 fluxes. Thus, even if the model is underrespresenting air-sea CO_2 fluxes over order 50% due to 50% biases in the estimation of mixed layer depth variability on seasonal to interannual timescales, the air-sea CO_2 fluxes will only make a minor contribution to the observed amplitude of variability at Mauna Loa.

5. Conclusions

[47] Two forced ocean model simulations were evaluated for the North Pacific in order to gain insight into the way in which anthropogenic CO_2 is taken up by the ocean. The simulations revealed that there is a wintertime "exchange window" for the anthropogenic component of air-sea CO_2 fluxes into the region where MLD is maximum in the mean (the region between 35–45°N and between 140–180°E) as well as the region near the southern margin of the subtropical gyre bounded by 10–20°N, 120–180°W. The amplitude of the uptake of the anthropogenic component of the air-sea CO_2 flux over the North Pacific is shown for the model to exhibit a positive trend over decadal timescales, with this largely reflecting increased uptake in winter.

[48] The basin-scale decadal trend in sea surface ΔpCO_2 simulated for the model is larger than the equivalent field identified in the data analysis study of *Takahashi et al.* [2006]. We interpret this difference between the model results and the data product of *Takahashi et al.* [2006] to reflect a bias in the observational record toward summer measurements. This implies that an observational network that tends to be biased toward summertime ΔpCO_2 measurements will lead to an inherent bias in inferred sea surface ΔpCO_2 trends and thereby underestimate the rate of uptake of anthropogenic CO_2 by the ocean. Thus it is imperative that future extensions of the observational network sample through the full seasonal cycle.

[49] The model also revealed that decadal trends in the large-scale circulation of the North Pacific contribute to the decadal trend in the large-scale structure of ΔpCO_2. Importantly, for the model it is the trends in the large-scale three-dimensional circulation of the gyres rather than one-dimensional processes (such as trends in local MLD) that drive the decadal trend in ΔpCO_2. In particular, the largest decadal trend in ΔpCO_2 is driven by a trend in the position of the boundary between the subpolar and subtropical gyres in the western and central parts of the basin. It is our hope that this study will motivate further process-oriented work on carbon cycle variability in and near the frontal region separating the subtropical and subpolar gyres.

[50] As the large-scale air-sea CO_2 fluxes in the model exhibit a pronounced seasonality for the Northern Hemisphere, we performed a calculation with an atmospheric transport model to evaluate the impact of this flux variability on atmospheric CO_2 concentrations at Mauna Loa. This calculation revealed that the air-sea fluxes drive relatively small variations of the CO_2 concentration on seasonal timescales, and that these changes are antiphased with respect to the observed seasonal cycle. The transport model also indicates that the ocean fluxes make only a very small contribution to the observed interannual variations in CO_2 concentration at Mauna Loa.

[51] **Acknowledgments.** We would like to thank John Dore for making his data available and the two anonymous reviewers for their constructive suggestions. This report was prepared by Keith B. Rodgers under award NA17RJ2612 from the National Oceanic and Atmospheric Administration, U.S. Department of Commerce. The statements, findings, conclusions, and recommendations are those of the authors and do not necessarily reflect the views of the National Oceanic and Atmospheric Administration or the U.S. Department of Commerce. This work was also supported by the European Northern Ocean Atmosphere Carbon Exchange Study (NOCES) project (EVK2-CT2001–00134). The calculations were performed on the NEC SX-5 at Institut du developpement et des resources en informatique scientifique (IDRIS) in France. We also thank the Ford Motor Company for their generous support.

References

Aumont, O., and L. Bopp (2006), Globalizing results from ocean in situ iron fertilization studies, *Global Biogeochem. Cycles*, *20*, GB2017, doi:10.1029/2005GB002591.

Bacastow, R. B., and E. Maier-Reimer (1990), Ocean-circulation model of the carbon cycle, *Clim. Dyn.*, *4*, 95–125.

Blanke, B., and P. Delecluse (1993), Variability of the tropical Atlantic ocean simulated by a general circulation model with two different mixed layer physics, *J. Phys. Oceanogr.*, *23*, 1363–1388.

Boyer, T. P., S. Levitus, J. Antonov, M. Conkright, T. O'Brien, and C. Stephens (1998), *World Ocean Atlas 1998*, vol. 5, *Salinity of the Pacific Ocean*, *NOAA Atlas NESDIS*, *30*, 166 pp., U.S. Gov. Print. Off., Washington, D. C.

de Boyer Montégut, C., G. Madec, A. S. Fischer, A. Lazar, and D. Iudicone (2004), Mixed layer depth over the global ocean: An examination of profile data and a profile-based climatology, *J. Geophys. Res.*, *109*, C12003, doi:10.1029/2004JC002378.

Dore, J. E., R. Lukias, D. W. Sadler, and D. M. Karl (2003), Climate-driven changes to the atmospheric CO_2 sink in the subtropical North Pacific Ocean, *Nature*, *424*, 754–757.

Gent, P. R., and J. C. McWilliams (1990), Isopycnal mixing in ocean circulation models, *J. Phys. Oceanogr.*, *20*, 150–156.

Gloor, M., E. Dlugokencky, C. Brenninkmeijer, L. Horowitz, D. F. Hurst, G. Dutton, C. Crevoisier, T. Machida, and P. Tans (2007), 3D SF6 data

and tropospheric transport simulations: 1. Signals, Modelling accuracy, Implications for inverse modeling, in revision, *J. Geophys. Res.*, *112*, D15112, doi:10.1029/2006JD007973.

Hack, J. J. (1994), Parameterization of moist convection in the NCAR community climate model (CCM2), *J. Geophys. Res.*, *99*, 5551–5568.

Holstlag, A., and B. Boville (1993), Local versus nonlocal boundary-layer diffusion in a global climate model, *J. Clim.*, *6*, 1825–1842.

Horowitz, L. W., et al. (2003), A global simulation of tropospheric ozone and related tracers: Description and evaluation of MOZART, version 2, *J. Geophys. Res.*, *108*(D24), 4784, doi:10.1029/2002JD002853.

Kalnay, E. C., et al. (1996), The NCEP/NCAR reanalysis project, *Bull. Am. Meteorol. Soc.*, *77*, 437–471.

Keeling, C. D., and S. C. Piper (2000), *Interannual Variations of Exchanges of Atmospheric CO_2 and $^{13}CO_2$ With the Terrestrial Biosphere and Oceans From 1978 to 2000: III. Simulated Sources and Sinks*, 68 pp., *Ref. 00-14*, Scripps Inst. of Oceanogr., Univ. of Calif., San Diego.

Keeling, C. D., H. Brix, and N. Gruber (2004), Seasonal and long-term dynamics of the upper ocean carbon cycle at station ALOHA near Hawaii, *Global Biogeochem. Cycles*, *18*, GB4006, doi:10.1029/2004GB002227.

Le Quéré, C., J. C. Orr, P. Monfray, and O. Aumont (2000), Interannual variability of the oceanic sink of CO_2 from 1979 through 1997, *Global Biogeochem. Cycles*, *14*, 1247–1265.

Lin, S.-J., and R. B. Rood (1996), Multidimensional flux-form semi-Lagrangian transport schemes, *Mon. Weather Rev.*, *124*, 2046–2070.

Madec, G., P. Delecluse, M. Imbard, and C. Levy (1998), *OPA 8.1 General Circulation Model Reference Manual*, *Notes de l'IPSL*, *11*, 91 pp., Univ. Pierre et Marie Curie, Paris. (Available from http://www.lodyc.jussieu.fr/opa)

Maier-Reimer, E., and K. Hasselmann (1987), Transport and storage of CO_2 in the ocean: An inorganic ocean-circulation cycle model, *Clim. Dyn.*, *2*, 63–90.

McKinley, G. A., M. J. Follows, and J. Marshall (2004), Mechanisms of air-sea CO_2 flux variability in the equatorial Pacific and the North Atlantic, *Global Biogeochem. Cycles*, *18*, GB2011, doi:10.1029/2003GB002179.

McKinley, G. A., et al. (2006), North Pacific carbon cycle response to climate variability on seasonal to decadal timescales, *J. Geophys. Res.*, *111*, C07S06, doi:10.1029/2005JC003173.

Obata, A., and Y. Kitamura (2003), Interannual variability of air-sea exchange of CO_2 from 1961–1998 with a global ocean circulation biogeochemistry model, *J. Geophys. Res.*, *108*(C11), 3337, doi:10.1029/2001JC001088.

Raynaud, S., O. Aumont, K. B. Rodgers, P. Yiou, and J. C. Orr (2006), Interannual-to-decadal variability of North Atlantic air-sea CO_2 fluxes, *Ocean Sci.*, *2*, 43–60.

Rodgers, K. B., O. Aumont, G. Madec, C. Menkes, B. Blanke, P. Monfray, M. C. Orr, and D. P. Schrag (2004), Radiocarbon as a thermocline proxy for the eastern equatorial Pacific, *Geophys. Res. Lett.*, *31*, L14314, doi:10.1029/2004GL019764.

Roullet, G., and G. Madec (2000), Salt conservation, free surface and varying volume: A new formulation for Ocean GCMs, *J. Geophys. Res.*, *105*, 23,927–23,942.

Sabine, C. L., et al. (2004), The ocean sink for anthropogenic CO_2, *Science*, *305*, 367–371.

Sarmiento, J. L., J. C. Orr, and U. Siegenthaler (1992), A perturbation simulation of CO_2 uptake in an ocean general circulation model, *J. Geophys. Res.*, *97*, 3621–3645.

Seager, R., Y. Kushnir, N. H. Naik, M. A. Cane, and J. Miller (2001), Wind-driven shifts in the latitude of the Kuroshio-Oyashio Extension and generation of SST anomalies on decadal timescales, *J. Clim.*, *14*(22), 4249–4265.

Takahashi, T., J. Olafsson, J. G. Goddard, D. W. Chipman, and S. C. Sutherland (1993), Seasonal variation of CO_2 and nutrients in the high-latitude surface oceans: A comparative study, *Global Biogeochem. Cycles*, *7*, 843–878.

Takahashi, T., et al. (2002), Global air-sea CO_2 fluxes based on climatological surface ocean pCO_2, and seasonal biological and temperature effects, *Deep Sea Res., Part II*, *49*, 1601–1622.

Takahashi, T., S. Sutherland, R. A. Feely, and R. Wanninkhof (2006), Decadal change of the surface water pCO_2 in the North Pacific: A synthesis of 35 years of observations, *J. Geophys. Res.*, *111*, C07S05, doi:10.1029/2005JC003074.

Wanninkhof, R. (1992), Relationship between wind speed and gas exchange over the ocean, *J. Geophys. Res.*, *97*, 7373–7382.

Wetzel, P., A. Winguth, and E. Maier-Reimer (2005), Sea-to-air CO_2 flux from 1948 to 2003: A model study, *Global Biogeochem. Cycles*, *19*, GB2005, doi:10.1029/2004GB002339.

Winguth, A. M. E., M. Heimann, K. D. Kurz, E. Maier-Reimer, U. Mikolajewicz, and J. Segschneider (1994), El Niño-Southern Oscillation related fluctuations of the marine carbon cycle, *Global Biogeochem. Cycles*, *99*, 39–63.

Xie, P., and P. A. Arkin (1997), Global precipitation: A 17-year monthly analysis based on gauge observations, satellite estimations, and numerical model inputs, *Bull. Am. Meteorol. Soc.*, *78*, 2539–2558.

Yasuda, T., and K. Sakurai (2006), Interdecadal variability of the sea surface height around Japan, *Geophys. Res. Lett.*, *33*, L01605, doi:10.1029/2005GL024920.

Zhang, G. J., and N. A. McFarlane (1995), Sensitivity of climate simulations to the parameterization of cumulus convection in the Canadian climate centre general circulation model, *Atmos. Ocean*, *33*, 407–446.

O. Aumont, Centre IRD de Bretagne, 29280 Plouzané, France.

C. Crevoisier, Laboratoire de Météorologie Dynamique, CNRS, IPSL, Ecole Polytechnique, 91128 Paliseau Cedex, France.

C. de Boyer Montégut, Frontier Research Center for Global Change (FRCGC), JAMSTEC, Yokohama Institute for Earth Sciences, 3173-25 Showa-machi, Yokohama, Kanagawa 236-0001, Japan.

N. Metzl, LOCEAN/IPSL, UMR 7159, Université Pierre et Marie Curie, Case 100, 4 place Jussieu, 75252 Paris Cedex 05, France.

K. B. Rodgers and J. L. Sarmiento, Atmospheric and Ocean Sciences, Princeton University, Princeton, NJ 08544, USA. (krodgers@princeton.edu)